The origin of the allometric scaling of lung ventilation in mammals

Frédérique Noël,[1] Cyril Karamaoun,[1] Jerome A. Dempsey,[2] and Benjamin Mauroy[3]

[1] *Université Côte d'Azur, LJAD, Vader center, Nice, France*
[2] *John Rankin Laboratory of Pulmonary Medicine, Department of Preventive Medicine, University of Wisconsin School of Medicine, Madison, Wisconsin, USA*
[3] *Université Côte d'Azur, CNRS, LJAD, Vader center, Nice, France**

(Dated: June 29, 2021)

A model of optimal control of ventilation has recently been developed for humans. This model suggests that the localization of the transition between a convective and a diffusive transport of the respiratory gas determines how ventilation should be controlled to minimize its energetic cost at any metabolic regime. We generalized this model to any mammal, based on the core morphometric characteristics shared by all mammals' lungs and on their allometric scaling from the literature. Since the main energetic costs of ventilation are related to the convective transport, we prove that, for all mammals, the localization of the shift from a convective transport into a diffusive transport plays a critical role on keeping that cost low while fulfilling the lung function. Our model predicts for the first time the localization of the transition in order to minimize the energetic cost of ventilation, depending on the mammals' mass and on the metabolic regime. From that optimal localization, we are able to predict allometric scaling laws for both tidal volumes and breathing rates, at any metabolic regime. We ran our model for the three common metabolic rates – basal, field and maximal – and showed that our predictions reproduce accurately the experimental data available in the literature. Our analysis supports the hypothesis that the mammals' allometric scaling laws of tidal volumes and breathing rates at a given metabolic rate are driven by a few core geometrical characteristics shared by the mammals' lungs and by the physical processes of the respiratory gas transport.

In animals, cellular respiration refers to the aerobic oxidation of fatty acids and glucose that represents a major source of energy production [1]. Oxidative processes require oxygen to be brought from the atmosphere to each individual cell. In parallel, carbon dioxide, a major by-product of the cellular respiration, has to be removed from the tissues [2]. The capture and transport of oxygen and the removal of carbon dioxide is performed by the respiratory and circulatory system. The lung allows the transport of oxygen from the ambient air to the alveolar exchange surface, in contact with the blood network. Then, the circulatory system transports the oxygen from the lung exchange surface to the cells. Conversely, carbon dioxide is transported from the cells to the ambient air [3].

The lung has been selected and shaped by evolution to fulfill the body needs in oxygen and to eliminate carbon dioxide [2]. The lung of mammals is composed of two main parts: the bronchial tree and the respiratory zone.

The bronchial tree is structured as a nearly dichotomous tree wherein an airflow circulates during the process of ventilation, which consists in a succession of inspiration and expiration cycles. At inspiration, fresh air is brought into the respiratory zone where oxygen exchange with the blood takes place. In parallel, carbon dioxide is transferred from the blood to the alveoli. Then, at expiration, a higher carbon dioxide/lower oxygen air is expelled from the lung [3].

The respiratory zone forms a large and thin exchange surface between the alveolar air and the blood. This surface is folded into the thorax cavity and connected to the ambiant air thanks to a compact bronchial tree. These characteristics have evolved to fulfill the gas exchange requirements in mammals while satisfying the structural body needs, namely a compact and rib-covered thorax cavity [4].

The transport of air in the lung by ventilation requires a certain amount of energy due to physical constraints, especially in the bronchial tree. A hydrodynamic resistance to the air flow in the bronchi arises from friction effects, due to air viscosity [5]. In parallel, mechanical energy is needed to expand the thoracic cage and the lung tissues during inspiration. That energy is lost at expiration by the viscoelastic recoil of the tissues, at least at rest [3]. Without a careful regulation, compensating these physical constraints could have a high metabolic cost, even at rest [6]. However, natural selection favors configurations that require low amounts or minima of energy. Moreover, the process of optimization by evolution is performed under the constraint of the lung's function: the gas exchange requirements have to fit metabolic activity.

The typical functional constraint associated to that energy cost was up to recently based on the total air flow rate entering the lung only [6–8], without accounting for the respiratory gas transport and the gas exchange requirements. More recently, Noël & Mauroy [9] optimized the energy spent for ventilation in humans with a more realistic functional constraint, based on the oxygen flow in the alveoli, including the physics of oxygen and carbon dioxide transport in a symmetric branched model of

* Corresponding author: benjamin.mauroy@unice.fr

the lung. This approach was not only able to predict physiological ventilation parameters for a wide range of metabolic regimes, but it also gave highlights on the distribution and transport of oxygen and carbon dioxide in the lung.

Actually, the progression of air in the lung is a combination of two mass transport processes: convection and diffusion. In the upper and central part of the bronchial tree, the convective transport largely dominates the mass transport, driven by the pressure gradient imposed by the airflow. However, as the cumulative surface of the bronchi section area increases at each bifurcation, the air velocity decreases while progressing towards the distal part of the tree. At some point, the characteristic velocity of convection becomes smaller than the characteristic velocity of diffusion; the mass transport becomes dominated by the diffusion process. The localization of the transition zone between convection and diffusion depends on the geometry of the lung and on the ventilation parameters. The previous work of Noël & Mauroy showed that the control of ventilation in humans localizes the transition zone as a trade-off between the oxygen demand and the availability and accessibility of the exchange surface deeper in the lung [9, 10].

The lungs of mammals share morphological and functional properties, raising the question on whether the previous results for human can be extended or not to all mammals. These properties are known to depend on the mass M of the animal, expressed in kg in this study, with non trivial power laws, called allometric scaling laws [2, 11–14]. The physics of ventilation, and hence its control, is linked to the geometry of the lung. Consequently, the morphological differences amongst mammals also affect the control of ventilation. This is supported by the allometric scaling laws followed by the ventilation frequency and tidal volume. Breathing rate at basal metabolic rate (BMR) has been estimated to follow the law $f_b^{\mathrm{BMR}} \simeq 0.58\ M^{-\frac{1}{4}}$ Hz [15] and tidal volume to follow the law $V_T^{\mathrm{BMR}} \simeq 7.14\ M^{1}$ mL [14, 16]. At other metabolic rates, less data is available in the literature except for the breathing rate of mammals at maximal metabolic rate (MMR), estimated to follow the law $f_b^{\mathrm{MMR}} \simeq 5.08\ M^{-0.14}$ Hz [17]. The links between these allometric scaling laws and the optimization of the energy spent for ventilation by mammals remains still to be uncovered. A model able to predict these laws for mammals would be a powerful tool to derive them at other regimes, such as at submaximal exercise, at maximal exercise or at field metabolic rate (FMR). Actually, the ventilation parameters at intermediate regimes are difficult to obtain, making the study of the metabolism of mammals at these regimes difficult to analyse [18]. Hence, a clear biophysical understanding of the origin of these scaling laws could allow to extend ventilation-related analyses performed for one mammal species to another. This could improve the pertinence of using animal models [19, 20] or, to the contrary, of using human data, richer in the literature, to understand other mammals' metabolism [16].

In this work, we develop two mathematical models: one to estimate the amount of oxygen captured from air by mammals lungs; and one to estimate the energetic cost of ventilation. These two models depend on the mass of the mammals and are coupled together to form a mathematical model for the natural selection of breathing rates and tidal volumes. Under our models hypotheses, we show that the physiological allometric scaling laws reported in the literature for both breathing rates and tidal volumes are actually minimizing the mechanical energy of breathing. Moreover, we show that the selected configurations at a given metabolic rate are mainly driven by the geometries of the mammals lungs and by the physical processes involved in oxygen transport in the lung.

MODELLING

The methodology and hypotheses used to build our analysis are summarised in Tables IV and V in Appendix A. The derivation of the allometric properties of ventilation is based on the previous model developed by Noël & Mauroy in [9], which is adapted to all mammals over 5 orders of magnitude in mass.

Ventilation pattern and energy cost of ventilation

The cost of ventilation is estimated as in [9] and its computation is based on [6–8]. The estimation of the cost is generalized to all mammals using allometric scaling laws for the mechanical parameters.

The velocity of the air entering the lung is represented using a sinusoidal pattern in time, i.e. under the form

$$u(t) = U \sin(2\pi t/T) \tag{1}$$

The quantity U is the maximal velocity and T is the period of ventilation, inverse of the breathing frequency $f_b = 1/T$. Denoting S_0 the surface area of the tracheal cross-section, the tidal volume is then $V_T = US_0T/\pi$, see Appendix B 1 and the air flow rate is $\dot{V}_E = V_T f_b$.

The biomechanics of the lung ventilation involves two active physical phenomena that are the sources of an energy cost [8, 9]. First, the motion of the tissues out of their equilibrium implies that the diaphragm has to use, during inspiration, an amount of energy that is stored in the tissues as elastic energy. This energy is then used during expiration for a passive recoil of the tissues. The power spent is related to the elastic properties of the thoracic cage and of the lung. These properties depend on the lung's compliance C [21] which is defined as the ratio between the change in volume of the lung and the change in pleural pressure. We derive the resulting power in Appendix B 2. Second, the airflow inside the bronchi induces an energy loss due to viscous effects that have to be compensated by the motion of the diaphragm during inspiration. The dissipated viscous power depends

on the hydrodynamic resistance R of the lung. Details about the derivation of the resulting power are given in Appendix B 3.

The total power $\tilde{\mathcal{P}}(V_T, f_b)$ spent by ventilation is the sum of these two powers

$$\tilde{\mathcal{P}}(V_T, f_b) = \underbrace{\frac{V_T^2 f_b}{2C}}_{\text{elastic power}} + \underbrace{\frac{1}{4}(\pi f_b V_T)^2 R}_{\text{viscous power}} \qquad (2)$$

The compliance and the hydrodynamic resistance of the lung follows allometric scaling laws that have been derived at BMR: $C \propto M^1$ [22] and $R \propto M^{-\frac{3}{4}}$ [14]. Nevertheless, the lung's volumes at exercise tend to stay within the linear part of the pressure–volume curve suggesting that the compliance does not change much at exercise [23]. Also, the diameters of the airways adjust during exercise and maintain the value of the lung's resistance near its rest level [24], see details in Appendix H. Hence, in our model, both the compliance and the hydrodynamic resistance are assumed independent of the metabolic regime. However, this hypotheses might not hold at very high exercise, where the power spent for ventilation is drastically increased due to non-linear responses. Hence, the previous hypotheses might underestimate the mechanical power needed for ventilation at intense exercise [25, 26].

The mechanical power has to be minimized with the constraint of an oxygen flow to the blood induced by the ventilation $f_{O_2}(V_T, f_b)$ matching the oxygen flow demand $\dot{V}_{O_2}$ of the metabolic regime considered. For a given mammal's mass, this formulates mathematically as searching for

$$\underset{(V_T, f_b)\in\mathcal{H}}{\text{Min}}\ \tilde{\mathcal{P}}(V_T, f_b) \quad \text{with } \mathcal{H} = \left\{(V_T, f_b)\,|\, f_{O_2}(V_T, f_b) = \dot{V}_{O_2}\right\} \qquad (3)$$

In the following, we will estimate the oxygen flow $f_{O_2}(V_T, f_b)$ transferred to the blood during the ventilation and the oxygen flow demand $\dot{V}_{O_2}$ according to the metabolic regime. Then, due to the complexity of the model, the optimization of the mechanical power will be carried out numerically. Our model will predict that the optimal tidal volume V_T and breathing rate f_b follow an allometric scaling law.

Core characteristics of the geometry of the mammals' lung

The lungs of mammals share invariant characteristics [35]. First, the lung has a tree-like structure with bifurcating branches. It decomposes into two parts: the bronchial tree or conductive zone that transports, mainly by convection, the (de)oxygenated air up and down the lung, and the acini or respiratory zone, where gas exchanges with blood occur through the alveolar–capillary membrane. The bronchial tree can be considered as self-similar, as the size of the branches is decreasing at each bifurcation with a ratio in the whole tree close to $h = \left(\frac{1}{2}\right)^{\frac{1}{3}}$ [4, 35, 36]. In the acini, the size of the branches are considered invariant at bifurcations [35, 37]. Thus, the bronchial tree is modelled as an airway tree with symmetric bifurcations [4, 9, 38, 39], as outlined in Figure 1. This model accounts for the branching pattern of the lung and for the lengths and diameters of the airways, but not for their spatial distribution. Actually, properties such as branching angles and orientations of the branching planes are not relevant in the model of oxygen transport developed in this work. Moreover, some mammals species have specific branching pattern [40**?**]. However, we only retain in our model the core property of the mammals lungs: the tree-like structure.

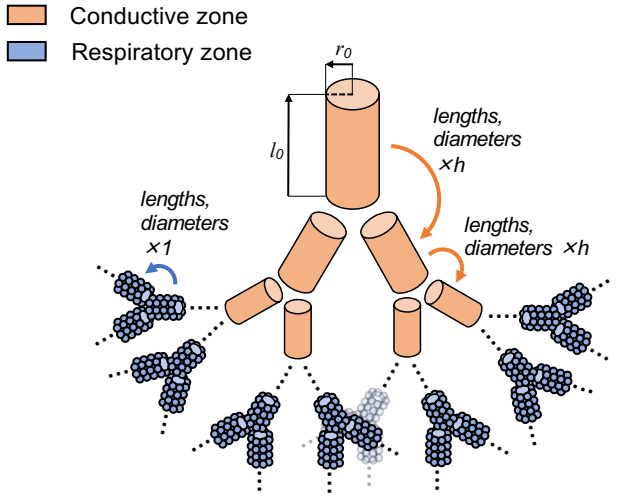

FIG. 1. Outlines of the lung's model used in this work. Our model is based on the assembly of selfsimilar trees with symmetric bifurcations that mimic the two functional zones. The tree in beige mimics the bronchial tree, where oxygen is only transported along the branches. The tree in blue mimics the acini, where oxygen is transported along the branches and also captured in the alveoli that cover the walls of the branches. The model for the physics of oxygen transport depends only on the lengths and diameters of the airways but not on their spatial distribution in the lungs. Hence, branching angles and branching planes orientations are not accounted for in this work.

A generation of the tree corresponds to the set of branches with the same number of bifurcations up to the trachea. The bronchial tree is modelled with G successive generations that connect to the acini that are modelled with H generations [35]. The total number of generations of the tree is then $N = G + H$. Hence, if the radius and length of the root of the tree, that mimics the trachea, are r_0 and l_0, the radius r_i and length l_i of an airway in

	Variables	Exponent		Prefactor
		Predicted [14]	Observed	
Morphometry	V_L: Lung volume	1	1.06 [22]	53.5 mL [22]
	r_0: Tracheal radius	3/8 (= 0.375)	0.39 [27]	1.83 mm*
	l_0: Tracheal length	1/4 (= 0.25)	0.27 [27]	1.87 cm*
	r_A: Radius of alveolar ducts	1/12 (≃ -0.083)	0.13 [28]	0.16 mm*
	l_A: Length of alveolar ducts	-1/24 (≃ -0.042)	N.D.	1.6 mm*
	n_A: Number of alveoli	3/4 (= 0.75)	N.D.	12 400 000*
	v_A: Volume of alveolus	1/4 (= 0.25)	N.D.	N.D.
Physics	f_b : Respiratory frequency (rest)	-1/4 (= -0.25)	-0.26 [22]	53.5 min^{-1} [22]
	V_T: Tidal volume (rest)	1	1.041 [14]	7.69 mL [22]
	P_{50}: O_2 affinity of blood	-1/12 (≃ -0.083)	-0.089 [29]	37.05 mmHg*
	R: Total resistance	-3/4 (= -0.75)	-0.70 [22]	24.4 $\text{cmH}_2\text{O}\ \text{s}\,\text{L}^{-1}$ [22]
	C: Total compliance	1	1.04 [22]	1.56 mL $\text{cmH}_2\text{O}^{-1}$ [22]
	P_{pl}: Interpleural pressure	0	0.004 [30]	N.D.

	Variables	Exponent at BMR	Exponent at FMR	Exponent at MMR
Metabolism	$\dot{V}_{O_2}$: O_2 consumption rate	3/4 (= 0.75) [13, 31]	0.64 [32]	7/8 (= 0.875) [33]
	t_c: Transit time of blood in pulmonary capillaries	1/4 (= 0.25) [14, 16]	1/4 (= 0.25) (hypothesized)	0.165 [16, 34]

TABLE I. Predicted and observed/computed values of allometric exponents for variables of the mammalian respiratory system. *: Prefactor computed using human values (M = 70 kg) at rest and computed for masses expressed in kg. BMR: Basal Metabolic Rate, FMR: Field Metabolic Rate, MMR: Maximal Metabolic Rate. N.D.: No data found.

generation i is

$$r_i = \begin{cases} r_0 h^i & i = 0...G-1 \\ r_{G-1} & i = G...N-1 \end{cases} \quad l_i = \begin{cases} l_0 h^i & i = 0...G-1 \\ l_{G-1} & i = G...N-1 \end{cases} \tag{4}$$

The dependence on the generation index of the airways surface areas S_i and of the mean air velocities u_i can be computed from the scaling laws on the airways radii, see Appendix B 4.

The derivation of a lung model that depends only on the mass requires to relate explicitly the morphological parameters involved in our model with the mass of the animal. We used the datasets from West et al. [14]. These authors derived for the cardiorespiratory system many theoretical allometric scaling laws that are in good agreement with the ecological observations.

The morphological parameters used in our model are the trachea radius r_0, the reduced trachea length l_0, the generations number G for the bronchial tree and H for the acini and the amount of exchange surface area per unit of alveolar duct wall surface area ρ_s. Each of these quantities follows an allometric scaling law that can be derived from [14]:

- The radius r_0 of the trachea scales as $M^{\frac{3}{8}}$ [14]. The bronchi radii, and consequently the dead volume, are affected by the ventilation regime [24, 43]. The airways' radii in our lung model are computed from the tree root radius r_0, see equation (4). Hence, the dependence on the metabolic rate of the dead volume is integrated into the prefactor of the tracheal radius allometric scaling law, see Appendix B 5.

- The allometric scaling law for the tracheal length $l_0 \propto M^{\frac{1}{4}}$ can be derived from [14], see Appendix B 6.

- Based on the hypothesis that the radii of the alveolar ducts are similar to the radii of the aveoli r_A [35] and on the allometric scaling law $r_A \propto M^{\frac{1}{12}}$ [14], we can deduce that $2^G \propto M^{\frac{7}{8}}$ and hence determine G, see Appendix B 7. Moreover, from [44, 45], we can assume that the number of generations of alveolar ducts H in the acini is independent of the mass and equal to 6.

- Then, relating the scalings of G and H to the allometric scaling law for the exchange surface area $S_A \propto M^{\frac{11}{12}}$ [14], we deduce that the amount of exchange surface per unit of alveolar duct surface ρ_s is independent of the mass, see Appendix B 8.

Hence, the number of airways generations $N = G + H$ predicted is about 13 for a 30 g mouse and about 23 for a 70 kg human, in agreement with physiological data [46, 47].

Oxygen transport and exchange with blood

The oxygen transport and exchange model in the human lung in [9] is extended to any mammal based on its mass M. The transport and exchange now occur in the idealized lung that has been generalized to any mammal in the previous section. The parameters of the transport and exchange model from [9] are also adjusted using relevant allometric scaling laws from [14].

The transport of oxygen in the lung is driven by three phenomena: convection by the airflow, diffusion and exchange with the blood through the alveoli walls. The mean partial pressure of oxygen over the section of a bronchus is transported along the longitudinal axis x of the bronchus. In the alveolar ducts, the exchange with blood occurs in parallel with the transport. Hence, in each airway belonging to the generation i, the partial pressure of the respiratory gas follows the convection–diffusion–reaction equation derived in [9] and in Appendix C,

$$\frac{\partial P_i}{\partial t} - \underbrace{D\frac{\partial^2 P_i}{\partial x^2}}_{\text{diffusion}} + \underbrace{u_i(t)\frac{\partial P_i}{\partial x}}_{\text{convection}} + \underbrace{\beta_i\left(P_i - P_{\text{blood}}\right)}_{\text{exchange with blood}} = 0, \quad \text{for } x \in [0, l_i], \quad (5)$$

where P_i is the mean oxygen partial pressure over the airway section, D is the oxygen diffusion coefficient in air and $u_i(t)$ is the mean air velocity in the airway of generation i. The reactive term β_i mimics the exchanges with the blood through the bronchi wall. β_i is equal to zero in the convective tree ($i = 0...G-1$) and is positive in the acini ($i = G...N-1$). In the acini, the oxygen exchange occurs through the wall of the ducts and β_i depends on the membrane and oxygen chemical properties, on the membrane thickness and on the local exchange surface derived from ρ_s, see Appendix B 8. More details about the derivation of β_i are given in Appendix C. As a consequence, the reaction term β_i follows an allometric scaling law, $\beta_i \propto M^{\frac{1}{12}}$, see Appendix B 9.

To determine the oxygen partial pressure in the blood that drives the oxygen exchange, we assume that the flow of oxygen leaving the alveolar duct through its corresponding exchange surface is equal to the flow of oxygen that is captured by the blood, accounting for the oxygen dissolved in the blood plasma and for the oxygen captured by the haemoglobin [9, 48], see Appendix D for more details.

The bifurcations are mimicked using boundary conditions that connect a generation to the next: we assume that the partial pressures are continuous at the bifurcations and that the amount of oxygen that goes through the bifurcation is conserved, see Appendix E.

Finally, the system is initialised at time $t = 0$ s using a distribution of partial pressure detailed in Appendix F.

With these hypotheses, our model takes as inputs the mass of the mammal M, the oxygen flow needed by the body $\dot{V}_{O_2}$, the tidal volume V_T and the breathing frequency f_b. The model outputs the flow of oxygen $f_{O_2}(V_T, f_b)$ exchanged with blood, see Appendix B 10.

Metabolic rate	Allometric scaling law	Reference
Basal (BMR)	$\dot{V}_{O_2}^{\text{BMR}} \propto M^{\frac{3}{4}}$	[13, 31]
Field (FMR)	$\dot{V}_{O_2}^{\text{FMR}} \propto M^{0.64}$	[32]
Maximal (MMR)	$\dot{V}_{O_2}^{\text{max}} \propto M^{\frac{7}{8}}$	[33]

TABLE II. Allometric scaling laws for mammals of the needed oxygen flow $\dot{V}_{O_2}$ at three metabolic rates. M is the mass of the mammal. Data from the literature.

Power optimization with a constrained oxygen flow

We will search the minimum of $\tilde{\mathcal{P}}(V_T, f_b)$ relatively to the tidal volume V_T and the breathing frequency f_b, see equation (2). The minimization is made with a constraint on the oxygen flow to the blood, written mathematically $f_{O_2}(V_T, f_b) = \dot{V}_{O_2}$. $f_{O_2}(V_T, f_b)$ is the oxygen flow to the blood resulting from a ventilation of the lung with the characteristics (V_T, f_b) and estimated with our model of oxygen transport and exchange in the mammals lung. $\dot{V}_{O_2}$ is the needed oxygen flow for the metabolic rate under consideration. Allometric scaling laws covering the whole set of mammals' species are available in the literature for basal, field and maximal metabolic rate, see table II. With these scalings, we can compute the desired oxygen flow $\dot{V}_{O_2}$ depending on the animal's mass M and metabolic regime. Other exponents for metabolic rates, less pertinent for our study, have also been derived for specific subsets of mammals' species, based for example on the size or on the athletic capacity [49, 50].

The model equations and the optimization process are performed as in [9], using numerical simulations. The numerical strategy is described in Appendix G and details about the sensitivity to the model parameters are given in Appendix H.

RESULTS

Our analysis assumes that, at the level of the mammals species, evolution selected for the minimum of the mechanical cost of ventilation, while allowing the lung to fulfil its functions of oxygen transfer to the blood.

Our modelling approach mimics this process and allows to determine optimal values for the breathing rate f_b and tidal volume V_T from the mass M of a mammal and from its metabolic regime. The mechanical power of ventilation $\tilde{\mathcal{P}}(V_T, f_b)$, estimated in equation (2), is optimized with a constraint on the oxygen flow. This functional constraint is expressed in our model as $f_{O_2}(V_T, f_b) = \dot{V}_{O_2}$. The oxygen flow $f_{O_2}(V_T, f_b)$ is computed using our model of oxygen transport and exchange in an idealised lung, see Figure 1 and equations (5). The quantity $\dot{V}_{O_2}$ is the targeted oxygen flow and corresponds

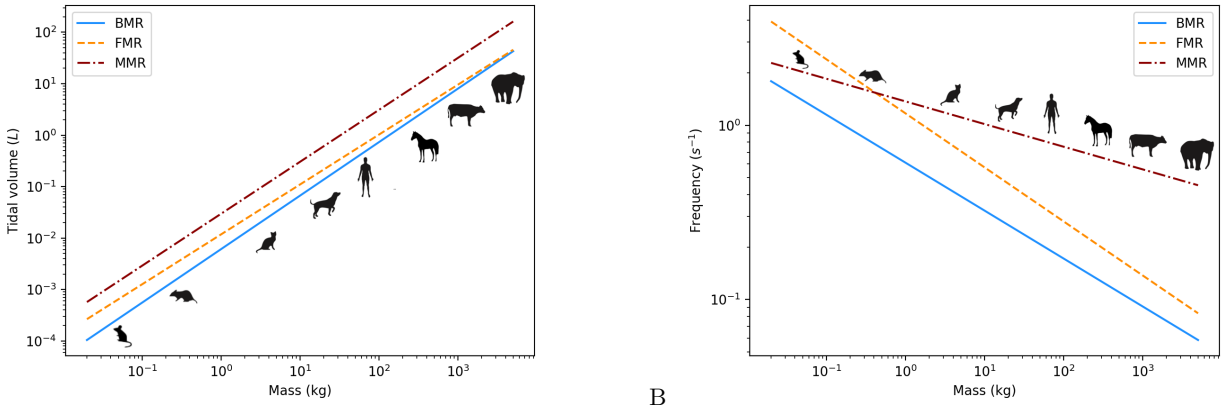

FIG. 2. **A:** Predicted tidal volume as a function of the mammals' mass (log-log). Solid line: BMR, $V_T^{\mathrm{BMR}} \simeq 6.1\ M^{1.04}$ ml; dashed line: FMR, $V_T^{\mathrm{FMR}} \simeq 11.8\ M^{0.97}$ ml, dash-dotted line: MMR, $V_T^{\mathrm{MMR}} \simeq 29.7\ M^{1.01}$ ml. **B:** Predicted breathing frequency as a function of the mammals' mass (log-log). Solid line: BMR, $f_b^{\mathrm{BMR}} \simeq 0.61\ M^{-0.27}$ Hz; dashed line: FMR, $f_b^{\mathrm{FMR}} \simeq 1.17\ M^{-0.31}$ Hz, dash-dotted line: MMR, $f_b^{\mathrm{MMR}} \simeq 1.37\ M^{-0.17}$ Hz. A larger dead volume at exercise [16] makes the oxygen source for diffusion slower to deplete. This might lead to a decrease in the optimal breathing rate, depending on the increase of the oxygen need. As a consequence, for small mammals, our model predicts breathing frequencies at MMR smaller than breathing frequencies at FMR.

to the mean oxygen demand for a mammal of mass M at the studied metabolic regime. Basal, field and maximal metabolic rates are analysed and the corresponding allometric scalings for $\dot{V}_{O_2}$ come from the literature, see Table II.

A synthesis of the hypotheses of our models is given in Appendix A in Table IV and V.

Allometric scaling laws of breathing rates and tidal volumes

In 1950, Otis et al. showed that by constraining the alveolar ventilation $\dot{V}_A = (V_T - V_D) f_b$ within $\tilde{\mathcal{P}}(V_T, f_b)$ with V_D being the dead volume, an optimal breathing frequency could be computed analytically [6, 8]. Using data available in the literature [12, 14, 16, 22] and the analytic formula from Otis et al., we derived allometric scaling laws for breathing frequency and tidal volume at BMR, $f_{b,\mathrm{pred}}^{\mathrm{BMR}} = 0.9\ M^{-\frac{1}{4}}$ Hz and $V_{T,\mathrm{pred}}^{\mathrm{BMR}} = 7.5\ M^{1}$ ml, see Appendix B 11. The allometric scaling laws computed are in good agreement with the observations, supporting the hypothesis of minimizing the mechanical power spent by ventilation. However, this approach is not able to predict the allometric laws at regimes other than BMR. Actually, the localization of the convection–diffusion transition in the lung drives the amount of oxygen flow to the blood [9]. Hence, only a model that is able to localize this transition in the tree and to compute precisely the amount of oxygen exchange would be able to reach satisfactory predictions.

Hence, we ran our model for the three metabolic regimes BMR, FMR and MMR. It predicts that the breathing rates and the tidal volumes follow allometric scaling laws in all the three regimes, see Figure 2,

$$\begin{aligned} f_b^{\mathrm{BMR}} &\simeq 0.61\ M^{-0.27}\ \mathrm{Hz}, \quad V_T^{\mathrm{BMR}} \simeq 6.1\ M^{1.04}\ \mathrm{ml} \\ f_b^{\mathrm{FMR}} &\simeq 1.17\ M^{-0.31}\ \mathrm{Hz}, \quad V_T^{\mathrm{FMR}} \simeq 11.8\ M^{0.97}\ \mathrm{ml} \\ f_b^{\mathrm{MMR}} &\simeq 1.37\ M^{-0.17}\ \mathrm{Hz}, \quad V_T^{\mathrm{MMR}} \simeq 29.7\ M^{1.01}\ \mathrm{ml} \end{aligned} \tag{6}$$

Our model predicts exponents that are in accordance with the values observed in the literature, see Table III. Moreover, the predicted prefactors show that our model is able to give quantitative predictions in accordance with the physiology.

	f_b (pred.)	f_b (obs.)	V_T (pred.)	V_T (obs.)
BMR	−0.27	−0.25	1.04	1
FMR	−0.31	N.D.	0.97	N.D.
MMR	−0.17	−0.14	1.01	N.D.

TABLE III. Predicted and observed exponents for the allometric scaling laws of the breathing frequency f_b and the tidal volume V_T at three different metabolic regimes [14–17], see equations (6).

Transition between convection and diffusion

The localization of the transition between convective and diffusive transport can be estimated with the Péclet number [9]. This number measures the relative influence of the transport of oxygen by convection over the transport by diffusion. The localization of the transition

zone corresponds to the generation i where the Péclet number, denoted Pe_i, becomes smaller than one, see Appendix B 12. The generation k at which the transition occurs depends on the mass and on the air flow rate $\dot{V}_E$, see Appendix B 13,

$$2^k \propto \begin{cases} \dot{V}_E^{\frac{3}{2}} \times M^{-\frac{3}{4}} & \text{if } k < G \\ \dot{V}_E \times M^{-\frac{5}{24}} & \text{if } k \geqslant G \end{cases} \tag{7}$$

At BMR, our model predicts that the convection–diffusion transition occurs within the convective tree for mammals with a mass larger than about 150 kg and within the acini for the others. The corresponding generation index k_{BMR} follows the law $2^{k_{\mathrm{BMR}}} \propto M^{0.405}$ if the mammal mass is larger than about 150 kg, and $2^{k_{\mathrm{BMR}}} \propto M^{0.56}$ otherwise. At MMR, the convection–diffusion transition always occurs in the acini at the generation index k_{MMR}, which follows the scaling $2^{k_{\mathrm{MMR}}} \propto M^{0.63}$. Hence, in each lung compartment, the location of the transition depends linearly on the logarithm of the animal mass, see Appendix B 14 and Figure 3.

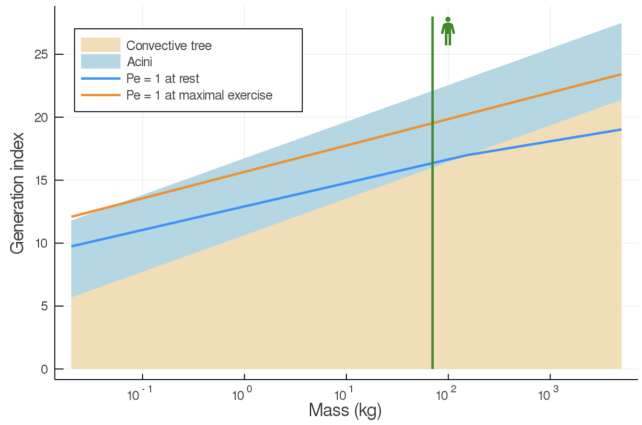

FIG. 3. Localization of the transition between a convective and diffusive transport of the oxygen in the lung as a function of the animal mass (logarithmic scale). The lines correspond to the localizations of that transition at BMR (rest, blue line) and MMR ($\dot{V}_{O_2}^{\max}$, orange line). The vertical green line corresponds to human mass (70 kg). The lower beige region corresponds to the convective zone of the lung, while the upper blue region corresponds to the exchange surface (acini). Small mammals tend to transport oxygen mainly by convection. Hence, there is no screening effect [10] affecting their exchange surface. Their oxygen pressure gradients between the alveoli and the blood are maximal everywhere, making their pulmonary system very efficient. To the contrary, due to the screening effect, large mammals use only a small portion of their exchange surface at rest. Hence, large mammals have a large reserve of exchange surface available for higher metabolic rates. By increasing the amplitude of ventilation, the screening effect is decreasing, making the large mammals pulmonary system more efficient at exercise than at rest.

At exercise, the transition occurs deeper in the lung of mammals than at rest. Animals with lower mass have a transition which is localized relatively deeper in their lung, as shown in Figure 3. In the acini, the oxygen is simultaneously displaced along the alveolar ducts and captured by the blood flowing in the alveoli walls. Consequently, the first alveolar ducts get higher oxygen concentration than those deeper. This phenomenon is known as the screening effect [10] and results in an exchange surface that can be only partly active, depending on the localization in the lung of the transition between convection and diffusion. Our model predicts that small mammals are using almost all the volume of their lungs at rest, with low screening effect. To the contrary, large mammals present a clear difference in term of volume usage between rest and exercise, with a transition localized near the end of the bronchial tree at rest, with strong screening effect, and a transition localized deeper in the acini at exercise, with a relatively lower screening effect.

Exhaled oxygen fraction

The oxygen flow captured by the lung is a proportion of the air flow inhaled, $\dot{V}_{O_2} = \dot{V}_E\ (f_I - f_E)$ with $\dot{V}_E = V_T f_b$ the air flow rate, f_I the oxygen fraction in ambient air and f_E the mean exhaled oxygen fraction. The allometric laws predicted by our model for tidal volumes and breathing rates allow to derive similar laws for the drop in oxygen fraction between ambient and exhaled air, $\Delta f = f_I - f_E$: $\Delta f^{\mathrm{BMR}} = 4.61\ M^{0.002}$ %, $\Delta f^{\mathrm{FMR}} = 5.02\ M^{-0.009}$ % and $\Delta f^{\mathrm{MMR}} = 5.12\ M^{0.0005}$ %. The drop in oxygen fraction depends only slightly on the mass and is in the range 3 to 5%, whatever the ventilation regime. With an inhaled oxygen fraction in air of about 21%, the oxygen fraction in the exhaled air is ranging from 16 to 18%, in full accordance with the physiology [35]. The quantity $\eta = \Delta f / f_I$ can be considered as a measure for the efficiency of oxygen extraction by the lung. Our model suggests that the system extraction is optimal for values of η of about 20%. Differences in η exists between small and large mammals because of the non zero exponents in the allometric scaling laws of Δf. However, the values of these exponents are small and cannot be interpreted as such. They might be the results of the simplifications made in the model and/or of the numerical approximations.

DISCUSSION

From a set of core morphometric parameters that represent the lung's geometry, our model allows to predict, at any metabolic regime, a set of dynamical parameters that represent the lung ventilation and that minimize an estimation of the mechanical cost of ventilation. This approach is able to predict with good accuracy the allometric scaling laws of mammals tidal volumes and breathing frequencies available in the literature (tidal volume at rest, breathing frequencies at rest and

$\dot{V}_{O_2}^{max}$ [14, 15, 17, 22, 51]). The validation of our model at both minimal and maximal metabolic regimes suggests that its predictions should be valid whatever the regime, in the limit of the availability of the input parameters. This indicates that the mechanical energy spent for ventilation might have driven the selection by evolution of the ventilation patterns.

The optimization process was functionally constrained, because the lung has to fulfil the function of transporting the needed respiratory gas to and from the blood. Although our model mimics only the function of transporting the oxygen, it is nevertheless able to reach valid predictions. This raises the question about the influence of other respiratory gases, and specifically, carbon dioxide. To answer this question, we adapted our model to account for a constraint on the flow of carbon dioxide, based on [9]. At rest, the new predictions were similar to that of a constrained oxygen flow. At exercise, we observed a shift between the two cases, with the constraint on oxygen flow leading to better predictions. This suggests that the oxygen flow could have driven the selection of the breathing rates and of the tidal volumes in mammals' species. This result might seem counterintuitive at first, as oxygen flow is suspected to have a low influence on the control of ventilation at the intraspecific level [52]. However, since the input of our model is the characteristic mass of a mammal species, our model is an interspecific model, and, as highlighted in the literature [53], interspecific and intraspecific levels can lead to drastically different behaviors. Finally, it is important to notice that, apart from the respiratory gas flows, other quantities, not accounted for in our model, are known to affect the control of ventilation such as mechanical, chemical or thermic regulations [43, 54, 55], at least at the intraspecific level.

The function of respiratory gas transport is dependent on the physical processes on which these transports rely. Except for small mammals, the most crucial physical phenomena is the screening effect [10]. Screening effect affects how the exchange surface is effectively used and drives at which depth in the lung the convection has to bring oxygen so that diffusion could take over the transport. The lung main response to change in the metabolic regime is to adjust the amount of exchange surface effectively used. Hence, only an analysis including a reliable representation of the mammal lung and of the gas transport is able to reach predictions compatible with the physiology whatever the regime.

The idealized representation of the bronchial tree and of the exchange surface used in this study accounts for five core characteristics common to all the mammals lungs, as identified in the literature [4, 6, 9, 14, 35]: a bifurcating tree structure; an homogeneous decrease of the size of the bronchi at the bifurcations; the size of the trachea; the size of the alveoli; and the surface area of the exchange surface. At a given metabolic rate, these characteristics are major determinants of the optimal tidal volume and breathing frequency that minimize the energetic cost of ventilation. This indicates that once the metabolic regime is fixed, the morphology of the lung is probably a core driver of the physiological control of ventilation. We tested this hypothesis by altering in our analysis the allometric scaling laws related to the geometry of the lung. We observed corresponding alteration of the laws predicted for tidal volumes and breathing frequencies. Since morphology itself has probably been selected by evolution in order to minimize the hydrodynamic resistance in a constrained volume [4, 56], morphology and ventilation patterns are intertwined together in order for the lung to function with a low global energetic cost, i.e. a low hydrodynamic resistance R and a low ventilation cost $\tilde{\mathcal{P}}(V_T, f_b)$ that also depends on R. Actually, this suggests that coevolution of these traits might have occurred in order to keep the cost of breathing as low as possible. Our representation of the lung does not account for interspecific differences known to exist between the lungs of mammals, such as different degrees of branching asymmetry, monopodial or bipodial lungs, etc. [37, 57–59]. Nevertheless, the predictions of our model for the localization of the convection–diffusion transition in idealized lungs lead to good estimations of the allometric scaling laws for tidal volumes and breathing frequencies, indicating that the morphological parameters included in our model might primarily drive the control of ventilation.

The generation index of the convection–diffusion transition, shown in Figure 3, depends linearly on the logarithm of the mass. Since the structure of the tree is also governed by allometric scaling laws, the generation index at which the transition between the bronchial tree and the acini occurs also depends linearly on the logarithm of the mass of the animal. However, the slopes are different and the convection–diffusion transition is located in the acini for small mammals and in the lower bronchial tree for large mammals. The reason is that larger mammals actually need less oxygen relatively to their mass than small mammals, as $\dot{V}_{O_2}/M \propto M^{-1/4}$ at rest and $\dot{V}_{O_2}^{max}/M \propto M^{-1/8}$ at $\dot{V}_{O_2}^{max}$. Hence, at rest, small mammals use almost all their exchange surface. They are subject to a low screening effect, making their lung non limitant, since it is able to respond efficiently to a change in metabolism. To the contrary, large mammals tend to use only a small portion of that surface at rest and are subject to a strong screening effect. Actually, the screened exchange surface in large mammals can be seen as an exchange surface reserve which can be recruited to allow higher metabolic rates. Interestingly, for masses near that of a human, the convection–diffusion transition at rest occurs near the beginning of the acini [9, 10, 36].

The ability to increase the metabolic rates plays a crucial role in animal life, for example for foraging or for responding to environmental threat. Our model suggests that the proportion of the oxygen extracted from the ambient air by the lung, found to be about 20%, depends only slightly on the metabolic regime. More oxygen can be extracted at higher metabolic regimes because the vol-

umes of inhaled air are larger. Except for small mammals, a larger volume of inhaled air allows to use a larger portion of the exchange surface, hence reducing *de facto* the screening effect and accelerating the exchange speed. As a consequence, the air has to be renewed at a quicker pace and breathing rate is increased. This last effect is however counterbalanced by the increase of the dead volume with the intensity of exercise [43]. However, the increase of the dead volume with the metabolic regime does not compensate the increase of the tidal volume. Typically our model predicts that, in humans, the ratio between both volumes falls from about 40% at BMR down to about 20% at MMR, in good agreement with the literature [16]. Nevertheless, larger dead volumes allow to bring a larger oxygen reserve at the convection–diffusion transition point. Hence relatively lower air renewing rates are needed. The optimization of the mechanical energy reflects the balance between the larger air volume and the air renewal rate needed to maintain an efficient oxygen diffusion gradient in the acini. Our model suggests that this effect plays an important role in the control of the breathing rates in small mammals. Instead, it predicts that small mammals should exhibit a breathing rate at MMR that is smaller than at FMR, as shown in Figure 2. Also, as small mammals exhibit almost no screening effect, the oxygen gradients between the alveoli and the blood are maximal everywhere in the acini and their lung is very efficient, whatever the regime [60]. This efficiency induces an optimal response of the lung to changes in the circulatory parameters and no reserve of exchange surface is needed. This brings up the hypothesis that the reserve of exchange surface may compensate the screening effect occurring in the lungs of large mammals. More specific studies and detailed analyzes of the respiratory system are however needed to confirm or infirm these predictions, in particular studies involving a more realistic coupling with the circulatory system.

Finally, there exists exceptions for which the oxygen demand can exceed the transport capacity of the lung at maximal exercise, such as in human highly trained endurance athletes or in thoroughbred horses [61, 62]. For these exceptions, the response of the control of ventilation induces increased airways resistances and flow limitations. As a consequence, the energy cost of ventilation becomes excessive for the metabolism. Our model could be used to study these configurations more specifically and bring insights on the physical processes involved in these limitations.

CONCLUSION

Our results highlight the influence of the transport of respiratory gas on the control of ventilation, and more generally, the behavior of the lung and respiratory system. Our results contribute to improve our understanding of the allometric scaling of ventilation in mammals. They represent a new theoretical framework explaining how the evolution might have driven the design of the respiratory system and its links with the organism metabolism. Our work suggests that the dynamical characteristics related to the control of ventilation is highly dependent on the morphological characteristics of the lung. This dependence comes from the physical processes involved in oxygen transport. Moreover, it has been suggested that several core morphological parameters related to the bronchial tree minimize the hydrodynamic resistance of the lung in a limited volume, so that the exchange surface can fill most of the thoracic space [4, 56]. Consequently, the control of ventilation is, at least partially, a direct consequence of the repartition of lung space between the bronchial tree and the acini. More generally, this highlights the importance of the geometrical constraints in the selection of organs characteristics, not only in terms of morphology, but also in terms of dynamics.

ACKNOWLEDGEMENTS

We would like to thank Dr. Elodie Vercken (INRAE, Institut Sophia Agrobiotech, France) for fruitful discussions. This work has been supported by the Agence Nationale de la Recherche, in the frame of the project VirtualChest (ANR-16-CE19-0014) and of the IDEX UCA JEDI (ANR-15-IDEX-01) and by the association Vaincre La Mucoviscidose (RF20190502489).

[1] H. Lodish, J. Darnell, A. Berk, P. Matsudaira, C. A. Kaiser, M. Krieger, M. P. Scott, and L. Zipursky, *Molecular Cell Biology*. W. H. Freeman, fifth edition ed., 2008.

[2] C. C. Hsia, D. M. Hyde, and E. R. Weibel, "Lung Structure and the Intrinsic Challenges of Gas Exchange," in *Comprehensive Physiology* (R. Terjung, ed.), pp. 827–895, Hoboken, NJ, USA: John Wiley & Sons, Inc., Mar. 2016.

[3] J. B. West, *Respiratory Physiology: The Essentials*. Philadelphia: Lippincott Williams and Wilkins, 9th revised edition ed., Aug. 2011.

[4] B. Mauroy, M. Filoche, E. R. Weibel, and B. Sapoval, "An optimal bronchial tree may be dangerous," *Nature*, vol. 427, pp. 633–636, Feb. 2004.

[5] B. Mauroy, *Viscosity : an architect for the respiratory system?* Habilitation à diriger des recherches, Université de Nice-Sophia Antipolis, Dec. 2014.

[6] A. B. Otis, W. O. Fenn, and H. Rahn, "Mechanics of Breathing in Man," *Journal of Applied Physiology*, vol. 2, pp. 592–607, May 1950.

[7] J. Mead, "Control of respiratory frequency," *Journal of Applied Physiology*, vol. 15, pp. 325–336, May 1960.

[8] A. T. Johnson, *Biomechanics and Exercise Physiology: Quantitative Modeling*. CRC Press, Mar. 2007. Google-Books-ID: oIvMBQAAQBAJ.

[9] F. Noël and B. Mauroy, "Interplay Between Optimal Ventilation and Gas Transport in a Model of the Human Lung," *Front. Physiol.*, vol. 10, 2019.

[10] B. Sapoval, M. Filoche, and E. R. Weibel, "Smaller is better—but not too small: A physical scale for the design of the mammalian pulmonary acinus," *PNAS*, vol. 99, pp. 10411–10416, June 2002.

[11] J. S. Huxley and G. Teissier, "Terminology of Relative Growth," *Nature*, vol. 137, pp. 780–781, May 1936.

[12] B. Gunther, "Dimensional analysis and theory of biological similarity," *Physiological Reviews*, vol. 55, pp. 659–699, Oct. 1975.

[13] R. H. Peters, *The ecological implications of body size*, vol. 2. Cambridge University Press, 1986.

[14] G. B. West, J. H. Brown, and B. J. Enquist, "A general model for the origin of allometric scaling laws in biology," *Science*, vol. 276, no. 5309, pp. 122–126, 1997.

[15] J. Worthington, I. S. Young, and J. D. Altringham, "The relationship between body mass and ventilation rate in mammals," *Journal of Experimental Biology*, vol. 161, pp. 533–536, Nov. 1991.

[16] H. C. Haverkamp, J. A. Dempsey, J. D. Miller, L. M. Romer, and M. W. Eldridge, "Physiologic responses to exercise," in *Physiologic basis of respiratory disease*, p. 17, Hamilton: BC Decker, Inc, 2005.

[17] J. D. Altringham and I. S. Young, "Power output and the frequency of oscillatory work in mammalian diaphragm muscle: the effects of animal size," *Journal of Experimental Biology*, vol. 157, pp. 381–389, May 1991.

[18] J. R. Speakman, "The history and theory of the doubly labeled water technique," *The American Journal of Clinical Nutrition*, vol. 68, pp. 932S–938S, Oct. 1998.

[19] G. Matute-Bello, C. W. Frevert, and T. R. Martin, "Animal models of acute lung injury," *American Journal of Physiology-Lung Cellular and Molecular Physiology*, vol. 295, pp. L379–L399, Sept. 2008. Publisher: American Physiological Society.

[20] P. R. M. Rocco and J. J. Marini, "What have we learned from animal models of ventilator-induced lung injury?," *Intensive Care Med*, pp. 1–4, June 2020.

[21] V. Agostini, E. Chiaramello, C. Bredariol, C. Cavallini, and M. Knaflitz, "Postural control after traumatic brain injury in patients with neuro-ophthalmic deficits," *Gait & Posture*, vol. 34, pp. 248–253, June 2011.

[22] W. R. Stahl, "Scaling of respiratory variables in mammals," *J. appl. Physiol*, vol. 22, no. 3, pp. 453–460, 1967.

[23] K. G. Henke, M. Sharratt, D. Pegelow, and J. A. Dempsey, "Regulation of end-expiratory lung volume during exercise," *Journal of Applied Physiology*, vol. 64, pp. 135–146, Jan. 1988. Publisher: American Physiological Society.

[24] B. D. Johnson, K. W. Saupe, and J. A. Dempsey, "Mechanical constraints on exercise hyperpnea in endurance athletes," *Journal of Applied Physiology*, vol. 73, pp. 874–886, Sept. 1992. Publisher: American Physiological Society.

[25] E. Agostoni and R. E. Hyatt, "Static Behavior of the Respiratory System," in *Comprehensive Physiology* (R. Terjung, ed.), Hoboken, NJ, USA: John Wiley & Sons, Inc., Jan. 2011.

[26] B. Mauroy, M. Filoche, J. S. Andrade, and B. Sapoval, "Interplay between geometry and flow distribution in an airway tree," *Physical Review Letters*, vol. 90, p. 148101, Apr. 2003.

[27] S. M. Tenney and D. Bartlett, "Comparative quantitative morphology of the mammalian lung: Trachea," *Respiration Physiology*, vol. 3, pp. 130–135, Oct. 1967.

[28] S. M. Tenney and J. B. Tenney, "Quantitative morphology of cold-blooded lungs: Amphibia and reptilia," *Respiration Physiology*, vol. 9, pp. 197–215, May 1970.

[29] D. S. Dhindsa, A. S. Hoversland, and J. Metcalfe, "Comparative studies of the respiratory functions of mammalian blood. VII. Armadillo (Dasypus novemcinctus)," *Respiration Physiology*, vol. 13, pp. 198–208, Nov. 1971.

[30] B. Günther and B. L. De la Barra, "Physiometry of the mammalian circulatory system," *Acta Physiologica Latino Americana*, vol. 16, no. 1, pp. 32–42, 1966.

[31] M. Kleiber, "Body size and metabolism," *Hilgardia*, vol. 6, pp. 315–353, Jan. 1932.

[32] L. N. Hudson, N. J. B. Isaac, and D. C. Reuman, "The relationship between body mass and field metabolic rate among individual birds and mammals," *Journal of Animal Ecology*, vol. 82, no. 5, pp. 1009–1020, 2013.

[33] E. R. Weibel and H. Hoppeler, "Exercise-induced maximal metabolic rate scales with muscle aerobic capacity," *Journal of Experimental Biology*, vol. 208, pp. 1635–1644, May 2005.

[34] C. M. Bishop and R. J. Spivey, "Integration of exercise response and allometric scaling in endotherms," *Journal of Theoretical Biology*, vol. 323, pp. 11–19, Apr. 2013.

[35] E. R. Weibel, *The Pathway for Oxygen: Structure and Function in the Mammalian Respiratory System*. Harvard University Press, 1984.

[36] C. Karamaoun, B. Sobac, B. Mauroy, A. V. Muylem, and B. Haut, "New insights into the mechanisms controlling the bronchial mucus balance," *PLOS ONE*, vol. 13, p. e0199319, June 2018.

[37] M. H. Tawhai, P. Hunter, J. Tschirren, J. Reinhardt, G. McLennan, and E. A. Hoffman, "CT-based geometry analysis and finite element models of the human and ovine bronchial tree," *J. Appl. Physiol.*, vol. 97, pp. 2310–2321, Dec. 2004.

[38] B. Mauroy, C. Fausser, D. Pelca, J. Merckx, and P. Flaud, "Toward the modeling of mucus draining from the human lung: role of the geometry of the airway tree," *Physical Biology*, vol. 8, p. 056006, Oct. 2011.

[39] B. Mauroy, P. Flaud, D. Pelca, C. Fausser, J. Merckx, and B. R. Mitchell, "Toward the modeling of mucus draining from human lung: role of airways deformation on air-mucus interaction," *Front. Physiol.*, vol. 6, 2015.

[40] O. Raabe, H. Yeh, G. Schum, and R. Phalen, "Tracheobronchial Geometry: Human, Dog, Rat, Hamster.," tech. rep., NM: Lovelace Foundation for Medical Education and Research, Albuquerque, 1976.

[41] J. N. Maina and P. van Gils, "Morphometric characterization of the airway and vascular systems of the lung of the domestic pig, Sus scrofa: comparison of the airway, arterial and venous systems," *Comparative Biochemistry and Physiology Part A: Molecular & Integrative Physiology*, vol. 130, pp. 781–798, Nov. 2001.

[42] R. J. Metzger, O. D. Klein, G. R. Martin, and M. A. Krasnow, "The branching programme of mouse lung development," *Nature*, vol. 453, pp. 745–750, June 2008.

[43] J. A. Dempsey and A. J. Jacques, "Respiratory System Response to Exercise in Health," in *Fishman's Pulmonary Diseases and Disorders* (M. A. Grippi, J. A. Elias, J. A. Fishman, R. M. Kotloff, A. I. Pack, R. M. Senior, and M. D. Siegel, eds.), New York, NY: McGraw-Hill Education, 5 ed., 2015.

[44] M. Rodriguez, S. Bur, A. Favre, and E. R. Weibel, "Pulmonary acinus: Geometry and morphometry of the peripheral airway system in rat and rabbit," *American Journal of Anatomy*, vol. 180, no. 2, pp. 143–155, 1987.

[45] B. Haefeli-Bleuer and E. R. Weibel, "Morphometry of the human pulmonary acinus," *Anat. Rec.*, vol. 220, pp. 401–414, Apr. 1988.

[46] R. F. Gomes and J. H. Bates, "Geometric determinants of airway resistance in two isomorphic rodent species," *Respiratory Physiology & Neurobiology*, vol. 130, pp. 317–325, June 2002.

[47] E. R. Weibel, A. F. Cournand, and D. W. Richards, *Morphometry of the Human Lung*. Springer, 1 edition ed., Jan. 1963.

[48] M. Felici, *Physics of the oxygen diffusion in the human lung*. PhD thesis, Ecole Polytechnique X, June 2003.

[49] C. R. White and R. S. Seymour, "Mammalian basal metabolic rate is proportional to body mass2/3," *Proc Natl Acad Sci U S A*, vol. 100, pp. 4046–4049, Apr. 2003.

[50] E. R. Weibel, L. D. Bacigalupe, B. Schmitt, and H. Hoppeler, "Allometric scaling of maximal metabolic rate in mammals: muscle aerobic capacity as determinant factor," *Respiratory Physiology & Neurobiology*, vol. 140, pp. 115–132, May 2004.

[51] I. S. Young, R. D. Warren, and J. D. Altringham, "Some properties of the mammalian locomotory and respiratory systems in relation to body mass," *Journal of Experimental Biology*, vol. 164, pp. 283–294, Mar. 1992.

[52] D. Robertshaw, "Mechanisms for the control of respiratory evaporative heat loss in panting animals," *Journal of Applied Physiology*, vol. 101, no. 2, pp. 664–668, 2006.

[53] L. Witting, *A general theory of evolution: by means of selection by density dependent competitive interactions*. Århus, Denmark: Peregrine Publisher, 1997. OCLC: 39246846.

[54] J. R. Speakman and E. Król, "The Heat Dissipation Limit Theory and Evolution of Life Histories in Endotherms—Time to Dispose of the Disposable Soma Theory?," *Integrative and Comparative Biology*, vol. 50, pp. 793–807, Nov. 2010.

[55] B. Sobac, C. Karamaoun, B. Haut, and B. Mauroy, "Allometric scaling of heat and water exchanges in the mammals' lung," *arXiv:1911.11700 [physics]*, Dec. 2019. arXiv: 1911.11700.

[56] X. Dubois de La Sablonière, B. Mauroy, and Y. Privat, "Shape minimization of the dissipated energy in dyadic trees," *Discrete and Continuous Dynamical Systems - Series B, American Institute of Mathematical Sciences*, 2011.

[57] B. Mauroy and P. Bokov, "The influence of variability on the optimal shape of an airway tree branching asymmetrically," *Phys Biol*, vol. 7, no. 1, p. 16007, 2010.

[58] M. Florens, B. Sapoval, and M. Filoche, "Optimal Branching Asymmetry of Hydrodynamic Pulsatile Trees," *Phys. Rev. Lett.*, vol. 106, p. 178104, Apr. 2011.

[59] A. Monteiro and R. L. Smith, "Bronchial tree Architecture in Mammals of Diverse Body Mass," *International Journal of Morphology*, vol. 32, pp. 312–316, Mar. 2014.

[60] R. F. Fregosi and J. A. Dempsey, "Arterial blood acid-base regulation during exercise in rats," *Journal of Applied Physiology*, vol. 57, pp. 396–402, Aug. 1984. Publisher: American Physiological Society.

[61] J. A. Dempsey, A. La Gerche, and J. H. Hull, "Is the healthy respiratory system built just right, overbuilt, or underbuilt to meet the demands imposed by exercise?," *Journal of Applied Physiology*, vol. 129, pp. 1235–1256, Dec. 2020.

[62] S. K. Powers, "Is the lung built for exercise?," *J Appl Physiol (1985)*, vol. 129, pp. 1233–1234, Dec. 2020.

[63] D. Elad, R. D. Kamm, and A. H. Shapiro, "Steady compressible flow in collapsible tubes: application to forced expiration," *Journal of Fluid Mechanics*, vol. 203, pp. 401–418, June 1989.

[64] P. T. MacKlem, "Physiology of Cough," *Ann Otol Rhinol Laryngol*, vol. 83, pp. 761–768, Nov. 1974. Publisher: SAGE Publications Inc.

[65] J. D. Anderson Jr, *Fundamentals of aerodynamics*. Tata McGraw-Hill Education, 2010.

[66] R. Hill, H. P. Wolvekamp, and F. G. Hopkins, "The oxygen dissociation curve of haemoglobin in dilute solution," *Proc. R. Soc. Lond. B*, vol. 120, no. 819, pp. 484–495, 1936.

[67] S. L. Lindstedt, "Pulmonary transit time and diffusing capacity in mammals," *American Journal of Physiology-Regulatory, Integrative and Comparative Physiology*, vol. 246, pp. R384–R388, Mar. 1984.

[68] J. Bezanson, A. Edelman, S. Karpinski, and V. B. Shah, "Julia: A fresh approach to numerical computing," *SIAM review*, vol. 59, no. 1, pp. 65–98, 2017. Publisher: SIAM.

Appendix

Appendix A: Strategy and models hypotheses

Table IV indicates the methodology used in our analysis. Table V on the next page describes the hypotheses of the two models coupled in our work.

Biological hypotheses [6–9]	
Evolutive hypothesis	We assume that, at the level of the mammals species, the ventilation parameters minimize the mechanical power of the ventilation.
Physiological constraint	We focus on the oxygen transport function of the lung and assume that the oxygen flow to the blood has to fit the metabolic regime.
Ventilation parameters	We characterize the ventilation with the breathing frequency f_b and the tidal volume V_T

Strategy	
Our analysis is based on **two input parameters**	• the mammal mass $\mathbf{M}$ • the metabolic need in term of oxygen flow $\dot{\mathbf{V}}_{\mathbf{O_2}}$, see Table II.
Oxygen flows at typical metabolic rates	The amount of oxygen flow needed by the metabolism follows allometric scaling laws that depend on the regime. • Basal Metabolic Rate (BMR): $\dot{V}_{O_2}^{\mathrm{BMR}} \propto M^{\frac{3}{4}}$ [13, 31] • Field Metabolic Rate (FMR): $\dot{V}_{O_2}^{\mathrm{FMR}} \propto M^{0.64}$ [32] • Maximal Metabolic Rate (MMR): $\dot{V}_{O_2}^{\max} \propto M^{\frac{7}{8}}$ [33]
Two mathematical models are used to compute estimations of physiological quantities	See details in Table V, the models inputs are M, $\dot{V}_{O_2}$ and the ventilation parameters $\mathbf{f_b}$ and $\mathbf{V_T}$ • the model 1 estimates the mechanical power to perform the ventilation of the lung $\tilde{\mathcal{P}}_{\mathbf{v}}(\mathbf{V_T}, \mathbf{f_b})$ • the model 2 estimates the oxygen flow from the lung to the blood network $\mathbf{f_{O_2}}(\mathbf{V_T}, \mathbf{f_b})$
The two models are used for a **constrained optimization process**	We search for the ventilation parameters $\mathbf{V_T}$ and $\mathbf{f_b}$ that minimize the mechanical power $\tilde{\mathcal{P}}_{\mathbf{v}}(\mathbf{V_T}, \mathbf{f_b})$ with the constraint $\mathbf{f_{O_2}}(\mathbf{V_T}, \mathbf{f_b}) = \dot{\mathbf{V}}_{\mathbf{O_2}}$ on the oxygen flow.

TABLE IV. General strategy and hypotheses.

Model 1: Power spent for lung ventilation, adpated from [6–9]

The mechanical power spent by lung ventilation has two main sources:
the air viscous dissipation in the airways and the elastic power stored in the thorax tissues

Model inputs:	Mammal mass M, tidal volume V_T and breathing rate f_b
Model output:	Mechanical power spent by the ventilation $\tilde{\mathcal{P}}_v(V_T, f_b)$
Viscous dissipation	Air viscous dissipation in the airways is estimated based on the hydrodynamic resistance of the lung, $R \propto M^{-\frac{3}{4}}$, see table I, Appendix B 3 and [22].
Elastic power	Elastic properties of the thorax and of the lung are estimated based on the compliance of the lung, $C \propto M^{1}$, see table I, Appendix B 2 and [22].

Model 2: Oxygen transport in the lung, adapted from [9]

Oxygen is transported in the airways by convection with air and by diffusion.
In the acini, oxygen is also exchanged with the blood through the airways wall.

Model inputs:	Mammal mass M, tidal volume V_T and breathing rate f_b
Model output:	Oxygen flow to the blood $f_{O_2}(V_T, f_b)$
Lung geometry	The topology of the geometrical model for the mammal lung is based on the literature [4, 35]. • The lung is modeled as a bifurcating tree where each airway is a cylinder. • The tree consists in two regions, a conducting zone and a respiratory zone. • The geometry of the bifurcations are neglected. The tree is scaled using scaling laws for mammals from the literature. • The root of the tree has a radius $r_0 \propto M^{\frac{3}{8}}$ [14] and a length $l_0 \propto M^{\frac{1}{4}}$, see Appendix B 6, the prefactor of r_0 accounts for the dependence of the dead volume on the metabolic regime, see Appendix B 5 and [24, 43]. • The size of the airways decreases at each bifurcation with a constant ratio $h = \left(\frac{1}{2}\right)^{\frac{1}{3}}$ in the conducting zone [4, 14] and remains the same in the respiratory zone, see Figure 1. • The conductive zone ends at generation index G when the radius of the smallest conductive airway reaches that of the alveoli radius, $r_A \propto M^{\frac{1}{12}}$, see Appendix B 7. • The number of generations H in the respiratory zone is assumed independent on the animal mass and equal to 6 [44, 45]. • The amount of exchange surface per airway in the respiratory zone ρ_S is determined based on the allometric scaling law on the exchange surface $S_A \propto M^{\frac{11}{12}}$, see Appendix B 8 and [14].
Air fluid dynamics	Our model uses the mean velocity of the air in the airways and accounts for the air flow conservation at each bifurcation [4, 9].
Oxygen transport	Oxygen transport occurs by convection with the air and by diffusion, see Appendix C [9]
Oxygen exchange with blood	As in [9], the physics of the oxygen exchange between the alveolar air and the blood is based on a diffusion process through a membrane. • The physical properties of the alveolar–capillary membrane is assumed to be equivalent to that of a water membrane. • The thickness of the alveolar–capillary membrane τ is assumed independent of the mass, $\tau \simeq 1\ \mu$m [10]. • The flow of oxygen through the membrane is assumed equal to the flow of oxygen stored by the blood flowing in the capillaries [9, 48], see Appendix E. • The blood flow follows an allometric scaling law based on the transit time of blood in the capillaries, see Appendix E.

TABLE V. Models hypotheses.

Appendix B: Details of the model computations

1. Tidal volume

The tidal volume is computed as the integral of the air flow $u(t)S_0$ over a half ventilation cycle,

$$V_T = \int_0^{\frac{T}{2}} S_0 u(t) \mathrm{d}t = \frac{U S_0 T}{\pi}$$

As $f_b = 1/T$, the parameterization is equivalent for (U, T) and (V_T, f_b).

2. Power associated to the compliance of the lung

The compliance is estimated by the ratio between the shift V in lung volume from functional residual capacity (FRC) and the corresponding shift in pleural pressure p_{pl}. The elastic energy stored is then $\mathcal{E}_e = \frac{1}{2} p_{pl} V = \frac{1}{2} \frac{V^2}{C}$. Finally, the instantaneous elastic power is $\frac{d\mathcal{E}}{dt} = \frac{1}{C} V(t) \frac{dV}{dt}$ with $V(t) = \int_0^t S_0 u(\xi) d\xi$. We recall that $u(t)$ is a sine function, see equation (1). Assuming that the elastic power is stored during inspiration only, its averaged value over a ventilation cycle is

$$\mathcal{P}_e(U, T) = \frac{1}{T} \int_0^{\frac{T}{2}} \frac{1}{C} V(t) \frac{dV}{dt}(t) \mathrm{d}t = \frac{1}{C} \frac{U^2 S_0^2 T}{2\pi^2}$$

Using the variables f_b and V_T leads to $\tilde{\mathcal{P}}_e(V_T, f_b) = \frac{V_T^2 f_b}{2C}$.

3. Power associated to the hydrodynamic resistance of the lung

The hydrodynamic resistance of the airway tree R is the ratio between the air pressure drop Δp applied between the root and the leaves of the tree and the resulting total air flow going through that tree Φ. The instantaneous power relative to the viscous dissipation in the airway tree is then $\Delta p \; \Phi = R\Phi^2$. In our model, $\Phi(t) = u(t)S_0$ with $u(t)$ the sine function defined in equation (1). Finally, we average the instantaneous power over a ventilation cycle assuming that the power is spent only during inspiration,

$$\mathcal{P}_v(U, T) = \frac{1}{T} \int_0^{\frac{T}{2}} R(u(t)S_0)^2 \mathrm{d}t = R \frac{U^2 S_0^2}{4}$$

Using the variables f_b and V_T leads to $\tilde{\mathcal{P}}_v(V_T, f_b) = (\pi V_T f_b)^2 R/4$.

4. Airway surface area and velocity versus generation index

The cross-section surface area of a branch in the generation i is $S_i = \pi r_i^2$. In the model of the bronchial tree ($i = 0...G-1$), $S_i = h^{2i} S_0$, while in the model of the acini ($i = G...N-1$), $S_i = S_{G-1}$. Air is assumed incompressible in the lung under normal ventilation conditions [63], except perhaps during cough [64]. This hypothesis is justified by the value of the air Mach number Ma in the lung. This number is computed with $Ma = U/c$, where U is the maximal velocity in the airways –reached in the trachea–, and c the speed of sound in air. The speed of sound in air is $c = \sqrt{1.4P/\rho}$ with $\rho \simeq 1.2$ kg.m^{-3} the density of the air and P the absolute pressure in the lung that can be considered in the range 1000 ± 100 cmH$_2$O at the different regimes studied in this work. Hence, for air velocities U below 100 m.s^{-1} (or air flow in the lung below 25 L/s), the Mach number remains below 0.3, which is a typical threshold for considering that compressible effects are negligible [65]. Consequently, the flow conservation leads to

$$u_i(t) = \begin{cases} u(t) \left(\frac{1}{2h^2}\right)^i & \text{for } i = 0...G-1 \\ u_{G-1}(t) \left(\frac{1}{2}\right)^{i-G+1} & \text{for } i = G...N-1 \end{cases}$$

5. Tracheal radius

From [14], the tracheal radius scales as $r_0 = aM^{\frac{3}{8}}$. The prefactor a depends on the metabolic rate and is determined based on human data and dead volumes: $a = 1.83\ 10^{-3}$ at BMR, $a = 1.93\ 10^{-3}$ at FMR and $a = 2.34\ 10^{-3}$ at MMR.

6. Tracheal length allometric scaling law

In our model, the dead volume is proportional to the tracheal volume and $V_{\text{dead}} \propto M^1$ [27]. Then, $V_{\text{dead}} \propto \pi r_0^2 l_0 \propto M^1$ leads to $l_0 \propto M^{\frac{1}{4}}$.

7. Conductive airways generations

The computation of G is based on the hypothesis that the radius of the alveolar ducts are similar to the radius r_A of the alveoli [35], for which an allometric scaling law is known, $r_A \propto M^{\frac{1}{12}}$ [14]. The number of generations G of the bronchial tree is then obtained from $r_A = r_{G-1} = r_0 h^{G-1}$, and the number of terminal bronchioles follows

$$2^{G-1} \propto M^{\frac{7}{8}}$$

This last allometric scaling law can be rewritten in the form $G = \left[\frac{\log(r_A/r_0)}{\log(h)}\right] + 1 = \left[\frac{7}{8}\frac{\log(M)}{\log(2)} + \text{cst}\right] + 1$.

8. Total gas exchange surface of the lung

The total gas exchange surface of the lung $S_A \propto M^{\frac{11}{12}}$ [14] is distributed over the walls of the alveolar ducts. In our model, a single alveolar duct has a lateral surface $s_{\text{ad}} = 2\pi r_A l_A$ with $l_A = l_0 h^{G-1} \propto M^{-\frac{1}{24}}$, hence $s_{\text{ad}} \propto M^{\frac{1}{24}}$. The total surface of alveolar ducts in the idealized lung is then

$$S_{\text{ad}} = 2^G \sum_{k=0}^{H-1} 2^k s_{\text{ad}} = 2^G (2^H - 1) s_{ad} \propto M^{\frac{11}{12}}$$

Hence, the amount of exchange surface per unit of alveolar duct surface, $\rho_s = S_A/S_{\text{ad}}$ is such that the product $\rho_s(2^H - 1) \propto M^0$ is independent on the mass of the animal. The number of generations of alveolar ducts in the acinus is considered independent of the mass [44, 45]. Consequently, ρ_s is also independent on the mass in our model. Under these conditions, our model respects the allometric scaling law from the literature $S_A \propto M^{\frac{11}{12}}$.

9. Flow rate of oxygen partial pressure per unit length of alveolar ducts

The thickness of the alveolar–capillary membrane τ is assumed independent of the mass, $\tau \simeq 1\ \mu$m [10]. The diffusivity D_{O_2,H_2O} of the oxygen in the tissues can be approximated by its value in water [10]. The flow rate of the oxygen partial pressure per unit length of an alveolar duct is then

$$\begin{aligned}\beta_i \left(P_i - P_{\text{blood}}\right) &= \rho_s \frac{2\pi r_A}{\pi r_A^2} \kappa \sigma_{O_2,H_2O} \frac{D_{O_2,H_2O}}{\tau} \left(P_i - P_{\text{blood}}\right) \\ &= \rho_s \frac{2\kappa}{r_A} \alpha \left(P_i - P_{\text{blood}}\right)\end{aligned}$$

where κ is the ratio relating partial pressure of the gas to its concentration in water, σ_{O_2,H_2O} is the solubility coefficient of the gas in water and D_{O_2,H_2O} is the diffusion coefficient of the gas in water. The permeability of the alveolar membrane α is $\alpha = \sigma_{O_2,H_2O} \frac{D_{O_2,H_2O}}{\tau}$.

10. Total flow of oxygen exchanged with the blood $f_{O_2}(V_T, f_b)$

The estimation of the total flow of oxygen exchanged with the blood $f_{O_2}(V_T, f_b)$ is computed from an established ventilation cycle,

$$f_{O_2}(V_T, f_b) = \frac{2\pi r_A \alpha \rho_s}{T} \sum_{i=G}^{N-1} 2^i \int_{t_C}^{t_C+T} \int_0^{l_i} (P_i(t,x) - P_{\text{blood}}(t,x))\, \mathrm{d}x\, \mathrm{d}t \tag{B1}$$

with t_C a time at which the system has reached a periodic regime and $T = 1/f_b$.

11. Otis et al. optimal breathing frequency at rest

The optimal breathing frequency computed by Otis et al. was obtained by canceling the derivative of the power relatively to f_b [6, 8],

$$f_{b,\text{pred}} = \frac{2\dot{V}_A/V_D}{1 + \sqrt{1 + 4\pi^2 RC\dot{V}_A/V_D}}. \tag{B2}$$

At BMR, the allometric scaling laws of all the physiological quantities involved in this expression for f_b are available in the literature: $\dot{V}_A \propto M^{\frac{3}{4}}$ [12], $V_D \propto M^1$ [22], $R \propto M^{-\frac{3}{4}}$ [14, 22] and $C \propto M^1$ [22]. Hence we are able to derive an allometric scaling law for breathing rate at BMR, f_b^{BMR}, based on ventilation data in healthy young humans [16],

$$f_{b,\text{pred}}^{\text{BMR}} = 0.9\ M^{-\frac{1}{4}}\ \text{Hz}$$

Based on the breathing frequency and, still, on the ventilation data from [16], we can deduce the allometric scaling law for the tidal volume at BMR, $V_T^{\text{BMR}} = \dot{V}_A/f_b^{\text{BMR}} + V_D$. Since $\dot{V}_A/f_b^{\text{BMR}} \propto M^{\frac{3}{4}}/M^{-\frac{1}{4}}$ and $V_D \propto M^1$, we have

$$V_{T,\text{pred}}^{\text{BMR}} = 7.5\ M^1\ \text{ml}$$

12. Péclet number

The Péclet number is computed by rewriting the transport equations 5 in a dimensionless form,

$$\frac{2l_i^2}{DT}\frac{\partial P_i}{\partial s} - \frac{\partial^2 P_i}{\partial \xi^2} + \underbrace{\frac{l_i u_i(sT/2)}{D}}_{Pe_i(s)} \frac{\partial P_i}{\partial \xi} + \frac{\beta_i l_i^2}{D}(P_i - P_{\text{blood}}) = 0, \text{ for } \xi \in [0,1] \tag{B3}$$

The dimensionless time is $s = 2t/T$ with $T/2$ the inspiration or expiration time and the dimensionless space is $\xi = x/l_i$. We define Pe_i as the average of the time-dependent Péclet number $Pe_i(s)$ over a half breath cycle. Then, for $i < G$,

$$\text{Pe}_i = \frac{2}{T}\int_0^{T/2} Pe_i(t)\mathrm{d}t = \frac{2V_T f_b l_0}{\pi r_0^2 D}\left(\frac{1}{2h}\right)^i$$

and for $i \geqslant G$,

$$\text{Pe}_i = \frac{2}{T}\int_0^{T/2} Pe_i(t)\mathrm{d}t = \frac{2V_T f_b l_0}{\pi r_0^2 D}\left(\frac{1}{2h}\right)^{G-1}\left(\frac{1}{2}\right)^{i-G+1}$$

.

13. Generation k of transition between convection and diffusion

The generation k at which the transition between convection and diffusion occurs is computed by solving the equation $\text{Pe}_\text{k} = 1$. If $k < G$, we have,

$$2^k = \left(\frac{2V_T l_0 f_b}{\pi r_0^2 D}\right)^{\frac{3}{2}} = \left(2\dot{V}_E \frac{l_0}{\pi r_0^2 D}\right)^{\frac{3}{2}} \propto \dot{V}_E^{\frac{3}{2}} \times M^{-\frac{3}{4}}$$

and if $k \geqslant G$,

$$2^k = \frac{2V_T l_0 f_b}{\pi r_0^2 D} \left(2^{G-1}\right)^{\frac{1}{3}}$$
$$= 2\dot{V}_E \frac{l_0}{\pi r_0^2 D} \left(2^{G-1}\right)^{\frac{1}{3}} \propto \dot{V}_E \times M^{-\frac{5}{24}}$$

14. Localization of the transition from convective to diffusive transport at BMR and MMR

At BMR, the generation index k_{BMR} at which the transition between a transport by convection and a transport by diffusion is localized depends on the metabolic rate and on the mass of the mammal,

$$k_{\mathrm{BMR}} = \begin{vmatrix} G - 1 + 3.41 - 0.47 \frac{\log(M)}{\log(2)} & (M \geqslant 154\,\mathrm{kg}) \\ G - 1 + 2.27 - 0.31 \frac{\log(M)}{\log(2)} & (M \leqslant 154\,\mathrm{kg}) \end{vmatrix}$$

The transition occurs in the convective tree for mammals with a mass larger than 154 kg and in the acini for mammals with a mass lower than 154 kg. In each compartment, the index depends linearly on the logarithm of the mass of the animal.

At MMR, the transition always occurs in the acini and the corresponding generation index k_{MMR} depends linearly on the logarithm of the mass of the animal,

$$k_{\mathrm{MMR}} = G - 1 + 5.02 - 0.24 \frac{\log(M)}{\log(2)}$$

The dependence of the indices k_{BMR} and k_{MMR} on the masses of the mammals are plotted in Figure 3.

Appendix C: Model equations

The transport of oxygen and carbon dioxide in the lung is driven by three main phenomena: convection, diffusion and exchange with the walls in the acini. The airways are modelled as cylinders. In our model, airways and fluid properties are the same in all the branches with the same generation index, hence we can study only one airway in each generation. For the generation i, we define $C_i(t, x)$ as the mean oxygen concentration at time t over the slice of the cylinder located at the position x on the axis of the cylinder. Equivalently, we define the mean partial pressure $P_i(t, x)$, which is proportional to the mean oxygen concentration.

The equations of oxygen transport in a cylinder are derived using a mass balance for oxygen in a slice with thickness dx localized at the position x on the cylinder axis, as schematized in Figure 4.

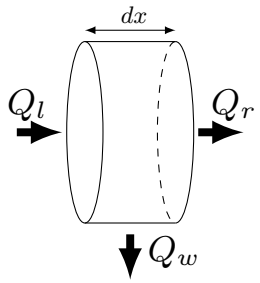

FIG. 4. Mass balance in a slice of an idealized airway (cylinder). The variation of the oxygen concentration in the slice depends on the balance between the oxygen flow entering the slice and getting out of the slice.

The quantity of oxygen entering the slice by the "left" side Q_l in Figure 4 is

$$Q_l(t, x) = \left(u_i(t) C_i(t, x) - D \frac{dC_i}{dx}(t, x)\right) \pi r_i^2$$

where D is the diffusion coefficient of oxygen in air, $u_i(t)$ is the mean velocity of the fluid in the generation i and r_i is the radius of the airways of generation i. The quantity of oxygen leaving the slice by the "right" side Q_r in Figure 4 is

$$Q_r(t,x) = -\left(u_i(t)C_i(t,x+dx) - D\frac{dC_i}{dx}(t,x+dx)\right)\pi r_i^2$$

Finally, the quantity of oxygen exchanged with the bronchus walls is

$$Q_w(t,x) = -\alpha_i \rho_s \left(P_i(x) - P_{\text{blood}}\right) 2\pi r_i dx$$

where P_{blood} is the O_2 partial pressure in the blood, ρ_s is the amount of exchange surface per unit of alveolar duct surface, see Appendix B 8, and α_i is the permeability of the alveolar membrane [48]:

$$\alpha_i = \begin{cases} 0 & (i = 0...G-1) \\ \alpha = \dfrac{D_{O_2,H_2O}\sigma_{O_2,H_2O}}{\tau} & (i = G...N-1) \end{cases} \tag{C1}$$

where D_{O_2,H_2O} is the diffusion coefficient of oxygen in water, σ_{O_2,H_2O} is the solubility coefficient of oxygen in water and τ is the thickness of the alveolar membrane.

Finally, the variation of the oxygen concentration over time in the slice is

$$\pi r_i^2 dx \frac{\partial C_i}{\partial t}(t,x) = Q_l(t,x) + Q_r(t,x) + Q_w(t,x)$$

Making the length of the slice dx go to zero, we obtain for $x \in [0, l_i]$,

$$\frac{\partial C_i}{\partial t}\pi r_i^2 - \underbrace{D\frac{\partial^2 C_i}{\partial x^2}\pi r_i^2}_{\text{diffusion}} + \underbrace{u_i(t)\frac{\partial C_i}{\partial x}\pi r_i^2}_{\text{convection}} + \underbrace{\alpha_i \rho_s \left(P_i - P_{\text{blood}}\right) 2\pi r_i}_{\text{exchange with blood}} = 0.$$

As the concentration and the partial pressure are proportional, we can work only with the partial pressure. Finally, the transport dynamics of the partial pressure of oxygen in a single branch is for $x \in [0, l_i]$,

$$\frac{\partial P_i}{\partial t} - \underbrace{D\frac{\partial^2 P_i}{\partial x^2}}_{\text{diffusion}} + \underbrace{u_i(t)\frac{\partial P_i}{\partial x}}_{\text{convection}} + \underbrace{\beta_i \left(P_i - P_{\text{blood}}\right)}_{\text{exchange with blood}} = 0 \tag{C2}$$

The exchange coefficient β_i is

$$\beta_i = \begin{cases} 0 & (i = 0...G-1) \\ \rho_s \dfrac{2k}{r_A}\alpha_i & (i = G...N-1) \end{cases} \tag{C3}$$

where k is the ratio relating the partial pressure of the oxygen to its concentration in water and r_A is the radius of the branches in the acinus.

Appendix D: Blood partial pressures

The blood partial pressure P_{blood} of oxygen depends non linearly on the local value of P_i, as a result of a balance between the amount of oxygen exchanged through the alveolar–capillary membrane and the amount of oxygen stored or freed during the passage of blood in the capillary [9].

As oxygen is stored within haemoglobin and dissolved in plasma, this balance writes

$$\alpha\left(P_i - P_{\text{blood}}\right) = 4Z_0(f(P_{\text{blood}}) - f(\tilde{P}_{aO_2})) + \sigma_{O_2} v_s \left(P_{\text{blood}} - \tilde{P}_{aO_2}\right) \tag{D1}$$

with Z_0 the haemoglobin concentration. Each of the haemoglobin molecule contains four sites of binding with oxygen molecules, hence the 4 in factor of Z_0. The function $f(x) = x^{2.6}/(x^{2.6}+26^{2.6})$ is the Hill's equation [66] that reproduces

the saturation of haemoglobin depending on the partial pressure of oxygen in blood. The quantity v_s corresponds to the blood velocity in the capillaries and σ_{O_2} corresponds to the solubility coefficient of oxygen in blood. The pressure $\tilde{P}_{aO_2} = 88$ mmHg is the effective partial pressure of oxygen in the arterial lung's circulation (low oxygenated blood) that accounts for potential previous visits of other alveoli by blood, as defined in [9]. This quantity is assumed independent on the mammal species [67].

The mean blood velocity v_s depends on the mass and on the metabolic regime studied. It can be computed as the ratio of the length of the capillary l_c over the transit time in the capillary t_c. As in [14], we assume that the terminal units of the blood network are invariant in size. Hence, the capillary length is fixed to a constant in our model and equals to 1 mm. The transit time in the capillaries depends both on the mass and on the metabolic regime,

$$\begin{aligned} t_c &\simeq 0.36\ M^{\frac{1}{4}} && \text{at basal metabolic rate [14, 16]} \\ t_c &\simeq 0.25\ M^{0.165} && \text{at maximal metabolic rate [16, 34]} \end{aligned}$$

No data is available in the literature for the field metabolic rate. Nevertheless, we determine a default allometric scaling law based on the fact that field metabolic rate [32] is more similar to basal metabolic rate than maximal metabolic rate for which the energy is mostly spent by muscle activity [16]. Hence, we assume that the exponent for t_c is the same at field metabolic rate and at basal metabolic rate.

Then, using the estimated value $t_c = 838$ s for human based on the data from Haverkamp et al. [16], we use as the allometric scaling law for the transit time at field metabolic rate,

$$t_c \simeq 0.29\ M^{\frac{1}{4}} \text{ at field metabolic rate}$$

Notice that the sensibility of our model relatively to that hypothesis is very low, as indicated in Appendix VI.

Appendix E: Boundary conditions

To mimic the bifurcations, we use the continuity conditions $P_i(l_i, t) = P_{i+1}(0, t)$ and the conservation of the number oxygen molecules

$$S_i \left(u_i(t) P_i(t, l_i) - D \frac{\partial P_i(t, l_i)}{\partial x} \right) - 2 S_{i+1} \left(u_{i+1}(t) P_{i+1}(t, 0) - D \frac{\partial P_{i+1}(t, 0)}{\partial x} \right) = 0 \tag{E1}$$

The 2 on the righthandside of the last expression indicates that an airway in the generation i divides into two airways in the generation $i + 1$.

The oxygen conversation can be rewritten, using the previous continuity condition,

$$-D S_i \frac{\partial P_i(t, l_i)}{\partial x} = -2 D S_{i+1} \frac{\partial P_{i+1}(t, 0)}{\partial x} \tag{E2}$$

Finally, we assume that $P_0(t, 0) = P_{\text{air}}$ at the trachea entrance, where P_{air} is the partial pressure of oxygen in the ambiant air. The surface area represented by the outlets of the deepest airways of the tree is negligible relatively to the whole exchange surface area. Moreover, the exchange occurring at these outlets is negligible relatively to the exchange occurring in the upper parts of the acini. Hence, we can assume that no exchange occurs at the outlets of the deepest airways in the acini, i.e. $-D \frac{\partial P_{N-1}}{\partial x}(l_A, t) = 0$.

Appendix F: Initial conditions

At time $t = 0$, we assume $u_i(0) = 0$, $\frac{\partial P_i}{\partial t}(0, x) = 0$ in the convective part of the tree ($i = 0...G-1$) and $P_i(0, x)$ constant in the acini ($i = G...N-1$). Then, an explicit stationary solution in the bronchial tree can be derived and used as a non trivial initial condition, for $i = 0...G-1$ with P_{blood} fixed to $\tilde{P}_{aO2} = 88$ mmHg (see Appendix III),

$$P_i(0, x) = P_{\text{air}} + \frac{P_{\text{blood}} - P_{\text{air}}}{\sum_{k=0}^{N} \left(\frac{1}{2h}\right)^k} \left(\sum_{k=0}^{i-1} \left(\frac{1}{2h}\right)^k + \left(\frac{1}{2h}\right)^i \frac{x}{l_i} \right).$$

For $i = G...N-1$, we suppose that the partial pressure is the same as the one in blood, $P_i(0, x) = P_{\text{blood}}$.

This initial condition allows to accelerate the algorithm by giving a non-trivial and physically relevant oxygen distribution at the start of the algorithm. Nevertheless, it is necessary to run the model of oxygen transport for several ventilation cycles to reach oxygen profiles in the airways that are periodic in time.

Appendix G: Numerical scheme

This model is analyzed with numerical simulations that allow to get numerical approximation of the solutions of the equations system. The numerical method is based on a discretization of the transport equations using an implicit finite differences scheme. The computation are performed using the computing language Julia [68]. From the initial distribution of partial pressures in the tree, the simulations are then run up to a time when the oxygen distribution pattern becomes periodic in time. All the model predictions are based on computations made when the oxygen profile is periodic.

The optimization process is made by inverting numerically the implicit constraint $f_{O_2}(V_T, f_b) = \dot{V}_{O_2}$ with the secant method. The inversion is equivocal and allows to compute numerically the non-linear function $f_b \to V_T(f_b)$. Then, the optimization is performed on the unidimensional function $f_b \to \tilde{\mathcal{P}}(V_T(f_b), f_b)$ by computing explicitly $\frac{d\tilde{\mathcal{P}}(V_T(f_b),f_b)}{df_b}$ from equation (2) and by solving $\frac{d\tilde{\mathcal{P}}(V_T(f_b),f_b)}{df_b} = 0$. The derivative $\frac{d\tilde{\mathcal{P}}(V_T(f_b),f_b)}{df_b}$ depends on $V_T(f_b)$ and $\frac{dV_T(f_b)}{df_b}$. The quantity $\frac{dV_T(f_b)}{df_b}$ is estimated numerically using the approximation $\frac{dV_T(f_b)}{df_b} = \frac{V_T(f_b+m)-V_T(f_b)}{m}$ with m a scalar small relatively to f_b.

Appendix H: Sensitivity analysis

Running sets of simulations, we studied the parameters sensitivity of our model, more specifically for the parameters where the data in the literature are scarce or missing.

First, our sensitivity analysis shows that our model has a very low sensitivity to the allometric scaling law of the blood residence time in the pulmonary capillaries, indicating that the choice made for the transit time of blood at field metabolic rate does not affect significantly the model predictions.

The hydrodynamic resistance R is positively correlated to the exponent of the breathing rate f_b. A hydrodynamic resistance independent on the ventilation regime leads to good predictions for the breathing rate at both BMR and MMR. This indicates that this hypothesis remains a good approximation. Moreover, it is supported by the physiological analyses in terms of change in dead volumes change and influence of inertia and turbulence [16], . Actually, if we neglect the inertia and turbulence in the bronchi at MMR, the change in dead volume at this regime leads the hydrodynamic resistance to be decreased by a factor larger than 3. In this case, the corresponding exponent for breathing rate drops to -0.10. Consequently inertia and turbulence might play an important role on the control of breathing rate, but, interestingly, their influence seems to be balanced by the increase of the dead volume.